atmosphere

Article

A 3D Monte Carlo Simulation of Convective Diffusional Deposition of Ultrafine Particles on Fiber Surfaces

Shixian Wu [1], Yongping Chen [1], Can Qi [1], Chunyu Liu [1], Gang Li [2] and Hui Zhu [1,*]

[1] School of Energy and Building Environment, Guilin University of Aerospace Technology, Guilin 541004, China
[2] Sinosteel Maanshan General Institute of Mining Research Co., Ltd., Maanshan 243000, China
* Correspondence: zhuhui@guat.edu.cn

Abstract: The microscale simulation of ultrafine particle transport and deposition in fibrous filtration media was achieved with a novel particle tracking model using a 3D Monte Carlo model. The particle deposition process is governed by the convection–diffusion field. Simulations were performed by considering the fibrous filtration media as an array of identical parallel fibers, in which the flow field was accurately described by an analytical solution. The model of particle movement was described by the random probability distribution characterized by a dimensionless factor, the Peclet number (*Pe*), based on a convection–diffusive equation of particle transport in fluid. The influence of the particle Peclet number (*Pe*) on the particle deposition process and the resulting deposition morphology was investigated. The results were analyzed in terms of dust layer growth, particles' trajectories and dust layer porosity for a vast range of Peclet numbers. The development of distinct deposition morphologies was found by varying the Peclet number (*Pe*). With a small Peclet number, diffusion dominated deposition and led to the formation of a more open and looser dust layer structure, while with larger Peclet numbers, convection dominated deposition and was found to form compact deposits. According to the change in the location of the packing densities along the dust layer height direction, the dust layer structure could be divided into three typical parts: the substructure, main profile and surface layer. In addition, the deposit morphologies observed for a high Pe were in good agreement with the experimental results found in the literature.

Keywords: fibrous filtration; particle deposition; convection-diffusion; dust layer; Monte Carlo simulation

check for updates

Citation: Wu, S.; Chen, Y.; Qi, C.; Liu, C.; Li, G.; Zhu, H. A 3D Monte Carlo Simulation of Convective Diffusional Deposition of Ultrafine Particles on Fiber Surfaces. *Atmosphere* **2022**, *13*, 1319. https://doi.org/10.3390/atmos13081319

Academic Editors: Xiaochuan Li and Gang Zhou

Received: 1 August 2022
Accepted: 16 August 2022
Published: 18 August 2022

1. Introduction

The impact of fine particulate matter has directly or indirectly caused serious environmental and health concerns such as hazy weather, acid rain and climate change owing to rapid economic development, industrial expansion and urbanization [1–3], and has led to great global concern. A bag filter based on the fiber filtration principle is an effective means of controlling particulate emissions with an overall mass filtration efficiency of >99% [4]. During the operation of a bag filter, the particles in the dust-laden gas will continuously be deposited on the surface of the filter material to form a dust layer, which causes a steep increase in pressure drop, meaning that additional energy will be consumed for sustaining the gas flow rate through the filter [5,6]. In order to optimize the design and operating conditions of the bag filter, it is necessary to obtain information on the dust layer morphology and the closely related filtration pressure drop.

In the past few decades, many theoretical and experimental studies have been carried out for understanding the deposition behavior of particles in fibrous filtration and the related components. Myojo et al. and Payatakes et al. observed the multi-mechanism deposition behavior of particles on a single fiber surface, considering the effects of convective diffusion, inertial collision and electrostatic fields [7–9]. Kasper et al. studied particle deposition on the surface of parallel fibers under inertial collision and rebound by a more elaborate experimental method, and quantitatively measured the porosity of the particle deposits [10,11]. Calle et al. and Song et al. investigated the relationship between the filtration pressure drop and the amount of deposition in fibrous filtration media from a macro perspective [12,13]. These experimental results confirmed that the filtration operating conditions play a crucial role in the evolution of the dust layer's morphology, which, in turn, affects the filtration characteristics.

Predictions of dust layer growth and the associated microstructure are often difficult to make, since they involve large-scale movements of the particle-laden host fluid and small-scale interactions (at the particle level). A set of analytical models of particle deposition on a single fiber for the period during which particle dendrites do not intermesh was developed by Payatakes [14,15]. However, these analytical models can only present phenomenological descriptions of dust layer growth, and are not capable of predicting the evolution of the deposits' structure and micromorphology. Computer modeling of this process has drawn great interest. There are two microscopic modeling techniques for modeling fine and ultrafine particles' transport and deposition controlled by Brownian diffusion and convection in fibrous filtration, namely Brownian Dynamics modeling (BD) and Monte Carlo techniques (MC). In the BD models, the particle motion information in a particle system is obtained by tracking the trajectory of an individual Brownian particle, which is determined by the well-known Langevin equation including the Gaussian distribution of the random force. The uniqueness of BD lies in its ability to account for timescale separation, allowing the consideration of complicated mechanical behavior, e.g., van der Waals forces between the surfaces of the particles and the collector or between particles, as well as external forces [16–20]. However, the BD technique requires the time step to be much smaller than the particle relaxation time in numerically integrating the Langevin equation for particle motion, requiring a high computational cost due to the small time step size.

The Monte Carlo (MC) method is a statistical simulation method for a direct approximate solution of the underlying microscale processes by using random numbers and probabilities [21]. Unlike conventional numerical methods, the Monte Carlo method uses probability density functions to directly simulate a system without requiring a complicated numerical solution, and thus much less computational cost is required compared with BD; hence, it has been successfully applied in the field of particle science. For example, Kanaoka et al. adopted a stochastic simulation method to simulate particles' deposition behavior on a single fiber surface under various deposition mechanisms, and a single fiber's collection efficiency was estimated on the basis of the simulation results [22–24]. Veerapaneni and Wiesner simulated the colloid deposition on a one-dimensional permeable surface from a uniform flow field by using Monte Carlo simulations, considering the effects of particle size, fluid velocity, and particle density on the transport of particles [25]. Rodríguez-Pérez et al. used an on-lattice dynamical Monte Carlo simulation for simulating particle deposit growth by advection–diffusion towards a 2D surface [26]. Song et al. developed a controlled kinetic Monte Carlo method based on classical kinetic Monte Carlo models to simulate nano-particle deposition processes in the field of thin film coating [27]. Höflinger and Jeon et al. developed a 2D computer simulation model for the compressible dust cake build-up on a model filter composed of an array of identical parallel fibers, and analyzed the local pore characteristics during the growth of the dust layer [28,29], but the convective diffusion of particles and the flow characteristics near the fibers were ignored; this model is therefore suitable for the deposition of larger particles without stochastic motion due to Brownian diffusion. Due to the geometrical constraints, these simulations performed in 2D space primarily provided qualitative insights into the real particle deposition process. Recently, some studies have applied 3D modeling to explore particles' deposition behavior in fibrous filtration in view of more realistic observations [30–33]. However, these studies treated the deposition surface and the closely related deposition morphology as simple collectors (e.g., a single fiber or a flat surface), which could not reproduce the real microstructure of particle deposition.

In the current study, in view of the convection–diffusion deposition of ultrafine particles in fibrous filtration, we extended our prior work on 2D space to 3D [34], in which the deposition surface was portrayed as a model filter composed of an array of identical parallel fibers instead of a single fiber or flat surface, and the flow field of the fibers was accurately described by an analytical solution. The objective of this study was to reveal the relationship between deposit morphology and the transport mechanism, followed by the structural evolution of dust layer described by the local porosity distribution. It is believed that the results predicted in this study can improve our understandings of particle deposition processes on the microscopic level, although the present model's application to actual processes is still limited.

2. Models and Methods

2.1. Physical Description and Assumptions

We considered the build-up of dust filter cakes on a three-dimensional model filter composed of an array of identical parallel fibers placed transverse to the flow, as shown in Figure 1a. The filtration media were represented by cylinders arranged in parallel, and the particles were generated randomly in the release surface and then moved towards filtration medium surface by convection–diffusion effects. When the distance between the center of the approaching particle and the fibers' surface was less than a particle radius or when the distance between the approaching particle and any deposited particles was less than the sum of the two particles' radii, the particle was considered to be deposited.

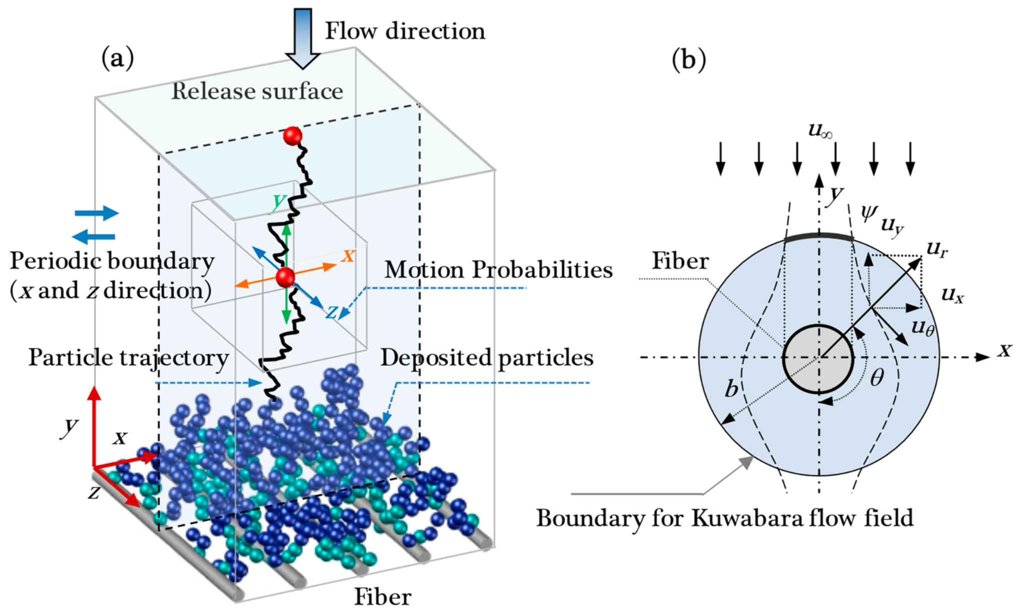

Figure 1. (**a**) Schematic of the simulation of a dust layer; (**b**) Kuwabara flow configuration.

In real dust filter cake growth, there are extremely complex mechanical behaviors including particle–particle, particle–filtration medium and particle–airflow interactions. To simplify the analysis, some assumptions were used in the calculations. These were as follows: (1) The particles entering the calculation area were assumed to be spherical with the same physical parameters. (2) Static electricity, gravity and other forces in the particles were assumed to not exist. (3) The effect of the dust layer on the flow field around the fibers was ignored. (4) The effect of inter-particle interaction forces on particle motion was ignored, and thus the dust cake was incompressible. (5) Only the deposition behavior of individual particles was considered in the particle motion calculations, and once an approaching particle had made contact with either any fibers or any previously deposited particles, it stuck to the collector (fibers or deposited particles) without rebounding. (6) There was a strong adhesive force between the particles to inhibit particle detachment due to aerodynamic forces, and thus a stable dust layer formed on the fibers' surface.

2.2. Model of Particle Motion

Based on the above physical assumptions, the transport equation for the particles deposition is given as

$$D\frac{\partial^2 n}{\partial x^2} + D\frac{\partial^2 n}{\partial y^2} + D\frac{\partial^2 n}{\partial z^2} - u_y\frac{\partial n}{\partial y} = 0 \tag{1}$$

The first three terms in Equation (1) are the diffusion terms in the x, y and z directions, and last term is the convective term in the y direction. In Equation (1), n is the number of particles per unit of volume at position (x, y, z), u_y is the migration velocity due to fluid drag at position (x, y, z) and D is the diffusion coefficient of particle, defined as [35]:

$$D = \frac{k_B T C_s}{3\pi\mu d_p} \tag{2}$$

where k_B is the Boltzmann constant and T is the absolute temperature, d_p is the particle diameter, μ is the dynamic viscosity of air and C_s is the Cunningham slip correction, which is taken to be [36]:

$$C_s = 1 + \frac{\lambda}{d_p}[2.514 + 0.8\exp(-0.55\frac{d_p}{\lambda})] \tag{3}$$

Here, λ is the mean free path of the surrounding fluid, which can be evaluated from the expression below [37]:

$$\lambda = kT/(\sqrt{2}\pi d_a^2 P) \tag{4}$$

where d_a is the diameter of air molecules and P is the fluid pressure.

In order to write Equation (1) in a dimensionless form, dimensionless variables were introduced as follows:

$$n^* = \frac{n}{n_0} x^* = \frac{x}{l} y^* = \frac{y}{l},\ z^* = \frac{z}{l} u_x^* = \frac{u_x}{u_\infty},\ u_y^* = \frac{u_y}{u_\infty} Pe = \frac{u_\infty l}{D}$$

where n_0 is the background particle number concentration in a gas to be purified, l is a characteristic length (l esd taken to be unity in the present simulations) and Pe is the Peclet number, a dimensionless parameter usually used to measure the relative importance of the diffusion mechanism and others in a mass transport process [38–40].

In this study, the Peclet number, Pe, was used to describe the ratio of convective movement (fluid velocity) to diffusive movement. By multiplying both sides of Equation (1) by $l^2/(D\ n_0)$, it may be rewritten in a dimensionless form as:

$$\frac{\partial^2 n^*}{\partial x^{*2}} + \frac{\partial^2 n^*}{\partial y^{*2}} + \frac{\partial^2 n^*}{\partial z^{*2}} - Pe(u_x^*\frac{\partial n^*}{\partial x^*} + u_y^*\frac{\partial n^*}{\partial y^*}) = 0 \tag{5}$$

In the Monte Carlo simulation of particle deposition, the particles' motion probabilities were derived from the macroscopic conservation equation, i.e., Equation (5). If δx^*, $\delta y^*$and δz^* are the step size in the x, y and z directions, respectively, then the discrete version of Equation (5) can be converted by the differential operators as follows:

$$\frac{\partial n^*}{\partial x^*} = (n^*_{x,y,z} - n^*_{x-1,y,z})/\delta x^* \tag{6a}$$

$$\frac{\partial n^*}{\partial y^*} = (n^*_{x,y,z} - n^*_{x,y-1,z})/\delta y^* \tag{6b}$$

$$\frac{\partial n^*}{\partial z^*} = (n^*_{x,y,z} - n^*_{x,y,z-1})/\delta z^* \tag{6c}$$

$$\frac{\partial n^*}{\partial x^{*2}} = (n^*_{x-1,y,z} + n^*_{x+1,y,z} - 2n^*_{x,y,z})/\delta x^{*2} \tag{7a}$$

$$\frac{\partial n^*}{\partial y^{*2}} = (n^*_{x,y-1,z} + n^*_{x,y+1,z} - 2n^*_{x,y,z})/\delta y^{*2} \tag{7b}$$

$$\frac{\partial n^*}{\partial z^{*2}} = (n^*_{x,y,z-1} + n^*_{x,y,z+1} - 2n^*_{x,y,z})/\delta z^{*2} \tag{7c}$$

By substituting Equations (6a)–(6c) and (7a)–(7c) into Equation (5), and imposing the condition of $\delta x^* = \delta y^* = \delta y^* = 1$, we obtain:

$$\begin{aligned} n^*_{x,y} &= \tfrac{n^*_{x+1,y,z}}{6+Pe(u^*_x+u^*_y)} + \tfrac{n^*_{x-1,y,z}(1+Peu^*_x)}{6+Pe(u^*_x+u^*_y)} + \tfrac{n^*_{x,y+1,z}}{6+Pe(u^*_x+u^*_y)} \\ &+ \tfrac{n^*_{x,y-1,z}(1+Peu^*_y)}{6+Pe(u^*_x+u^*_y)} + \tfrac{n^*_{x,y,z}}{6+Pe(u^*_x+u^*_y)} + \tfrac{n^*_{x,y,z}}{6+Pe(u^*_x+u^*_y)} \end{aligned} \tag{8}$$

If we apply the relationship between particle concentration and the probability of a particle moving in three-dimensional space to Equation (8), the probability of the particle moving in the six directions is [41,42]:

$$\begin{aligned} &P_{x+1,\ y,z} = \tfrac{1}{6+Pe(u^*_x+u^*_y)},\ P_{x-1,\ y,z} = \tfrac{1+Peu^*_x}{6+Pe(u^*_x+u^*_y)},\ P_{x,\ y+1,z} = \tfrac{1}{6+Pe(u^*_x+u^*_y)}, \\ &P_{x,\ y-1,z} = \tfrac{(1+Peu^*_y)}{6+Pe(u^*_x+u^*_y)},\ P_{x,\ y,z+1} = \tfrac{1}{6+Pe(u^*_x+u^*_y)},\ P_{x,\ y,z-1} = \tfrac{1}{6+Pe(u^*_x+u^*_y)} \end{aligned} \tag{9}$$

As can be seen from Equation (9), the motion probabilities depend upon the dimensionless parameter *Pe*. Under the limiting condition of $Pe \to 0$, the transport probability of particles in each direction will be 1/6, and the deposition behavior is reduced to the well-known diffusion-limited deposition [43,44]. On the other hand, for the case of $Pe \to \infty$, the diffusion effect is negligible, and convection is the dominant transport mechanism, i.e., the approaching particles follow the streamline exactly. In the middle region, the particles' motion is controlled by a combination of particle diffusion and convection. *Pe* can therefore be used to describe the relative importance of these two particle transport mechanisms (i.e., diffusion and convection).

Note that in Equation (9), the determination of the probabilities of particle motion requires knowledge of the local flow velocities (i.e., u_x*, u_y* and u_z*) in the simulation domain. In the present study, we restricted the analysis to the filtration at a low Reynolds number ($Re \ll 1$) and the simplified filter model as described in Figure 1, so the flow around the filtration medium can be considered to be creeping flow in two-dimensional space. In this case, the modified Kuwabara flow model including the slip effect at the fiber surface is valid [45,46] and can be used to estimate the flow velocity in proximity to a fiber. The flow field beyond the Kuwabara cell was assumed to be rectilinear for simplicity. In the polar coordinates in Figure 1b, the stream function Ψ for the Kuwabara model is described by:

$$\psi = \frac{2ur}{J}\left[A\left(\frac{r_{\mathrm{f}}}{r}\right)^2 + B + C\ln\left(\frac{r_{\mathrm{f}}}{r}\right) + D\left(\frac{r_{\mathrm{f}}}{r}\right)^2\right]\sin\theta \tag{10}$$

where:

$$A = c/2 - 1 - cKn,\ B = 1 - c,\ C = -4(1/2 + Kn),\ D = (1/2 + Kn)c,\ c = (r_{\mathrm{f}}/b)^2,\ Kn = \lambda/r_{\mathrm{f}}$$

and:

$$J = 3 + 2\ln c - 4c + c^2 + Kn(2 + 4\ln c - 2c^2)$$

where u is the mean velocity inside the filter,$u = u_\infty/(1-c)$, in m/s; u_∞ is the undisturbed approach velocity of the gas (i.e., the filtration velocity), in m/s, c is the packing density of the filter, defined as the ratio of the volume of the fibers to that of the Kuwabara cell; Kn is the Knudsen number; and b and r_{f} are the radius of the Kuwabara cell and the fiber, respectively (see Figure 1b).

With Cartesian coordinates, the velocity components of the Kuwabara flow field in the x and y directions are found by using [45]:

$$u_x = -\frac{r_f{}^2}{r^2 \sin\theta}\frac{\partial\psi}{\partial\theta},\ u_y = \frac{r_f{}^2}{r\sin\theta}\frac{\partial\psi}{\partial r},\ u_z = 0 \quad (11)$$

In the Monte Carlo simulations, the initial position of the individual approaching particle on the "release surface" located above the filtration medium was first assigned using a random number with a uniform deviation between 0 and 1 (see Figure 1). Once released, the particle was allowed to move in any of six directions in terms of the motion probabilities determined by Equation (9) at a given *Pe*, and thus its trajectory could be determined. The knowledge of the particle's trajectory, in turn, determined whether or not a given particle would be deposited and, if so, the deposition position. If a particle migrated outside the simulation domain in the x and z direction, it re-entered on the opposing side at the same height (i.e., periodic boundary conditions). If a particle migrated through the fiber layer, it was discarded from the simulation and a new particle was released. This procedure was repeated until the number of the deposited particles reached a preset value. A more detailed description of the simulation procedure can be seen in the flow chart (Figure 2).

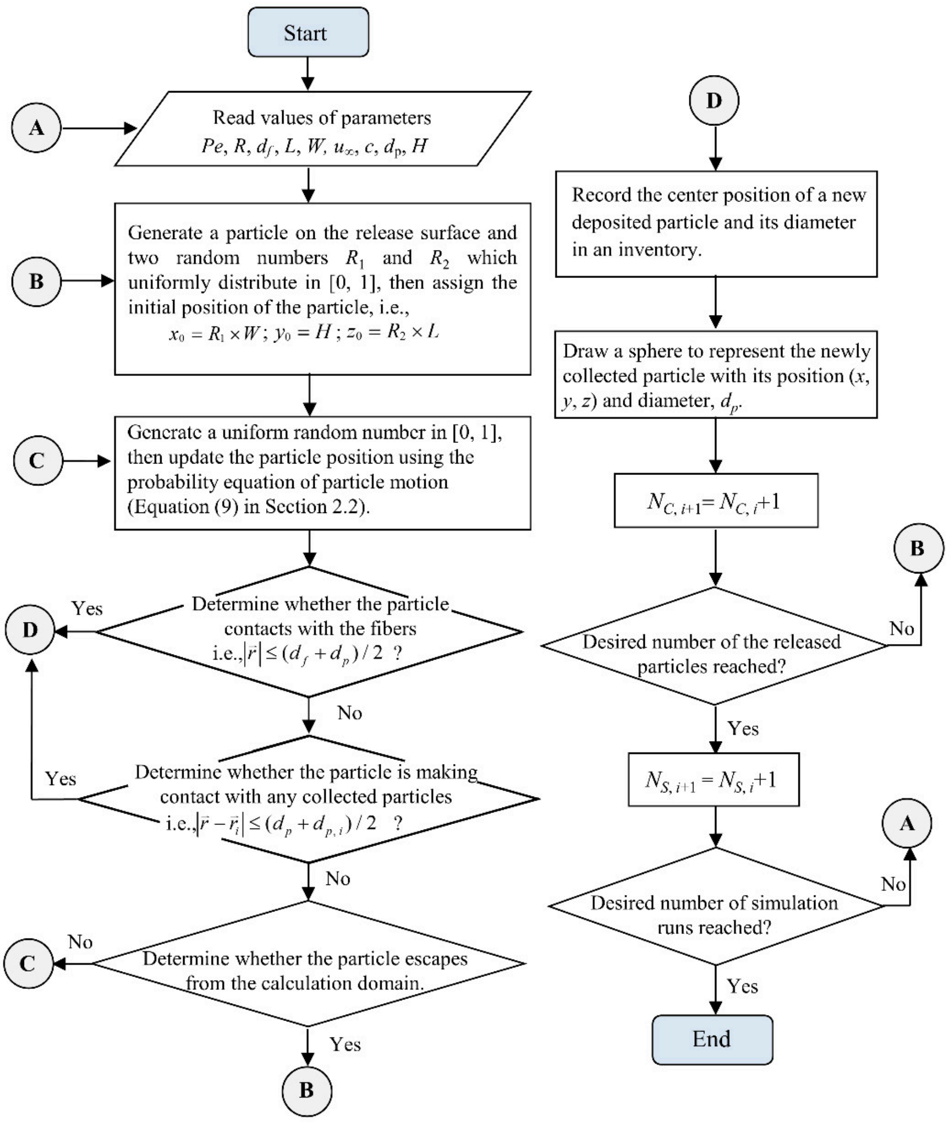

Note: N_C denotes the number of deposited particles, N_S denotes the number of released particles.

Figure 2. Flow chart of the simulation procedure.

3. Results and Discussion

3.1. Validation of the Computational Method

The numerical model used in this study was validated against the experimental observations given by Kanaoka et al., and Bhutra and Paratakes [47,48], and the results are shown in Figure 3. The conditions under which the simulations were made were identical to those used in the deposition experiments, and the specific parameters were as follows: (a) Case 1: u_∞ = 0.5 m/s, d_p = 1 μm, d_f = 10 μm, ρ_p = 11.34 g/cm^3, fiber length L_f = 50 μm, number of the deposited particles N_C = 800; (b) Case 2: u_∞ = 0.3 m/s, d_p = 3.3 μm, d_f = 25 μm, ρ_p = 0.66 g/cm^3, fiber length L_f = 125 μm, N_C = 300. The packing density of the fibrous filter was set to 0.001 (as an approximation of an isolated fiber used in the experiments) for both cases. For Case 1, the inertial effect of particles was significant due to their high density; the incoming particle moved almost in a straight-line trajectory until it contacted the fiber, and the effect of the flow field around the fiber on the particle's motion was negligible. However, for Case 2, the particle moved toward the fiber almost along the flow streamline due to the very low density; this case corresponded to the limiting condition of $Pe \rightarrow 0$, i.e., a purely convective transport mechanism. In a comparison of the simulation experiments, the straight-line and streamline trajectories were therefore applied for particle motion for Cases 1 and 2, respectively. Figure 2 shows that fairly good agreement on the morphology of particle deposition was obtained between the simulations and the experimental observations. The verifications confirmed that the proposed stochastic simulation model was capable of simulating particle deposition and then providing the particle deposition morphology. In addition, a comparison of the deposit morphologies between Case 1 and Case 2 suggested the possibility of the strong effects of the transport mechanism on the morphology of the deposits on the fibers' surface. This will be discussed in the next section in detail.

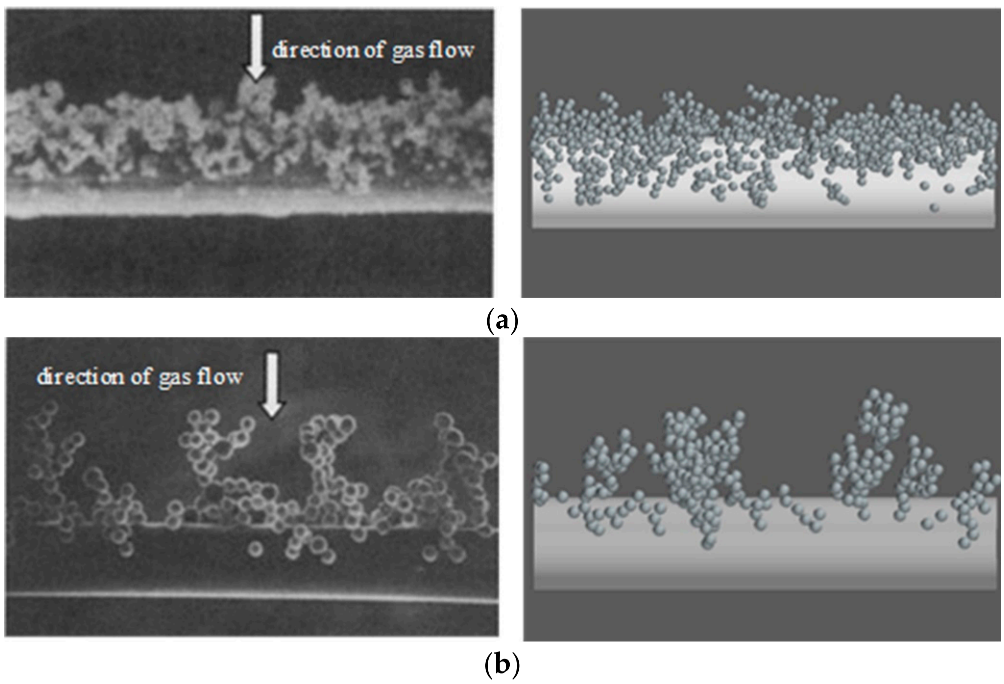

Figure 3. Comparisons of the deposit morphologies on a fiber between the simulations and the experimental observations. (**a**) Comparison of the simulation results in Case 1 with the experimental results of Kanaoka et al. [47]. (**b**) Comparison of the simulation results in Case 2 with the experimental results of Bhutra and Paratakes [48].

3.2. Dust Layer Growth

To investigate the effect of the abovementioned particle transport mechanism (measured by *Pe*) on the resulting microstructure of the dust layer, simulation runs were performed for different values of *Pe* with a range from 0.2 to 5000. The number of deposited particles *Nc* was set to 5000 for $Pe > 1$ and 2000 for $Pe \leq 1$ in order to reduce the computational time. In present study, for each case, at least five independent simulation runs were performed repeatedly for obtaining a meaningful ensemble average of the simulation results. The other simulation parameters used in the present study were as follows: filter packing density $c = 0.2$, i.e., the spacing between fibers was $5d_f$ (here, d_f denotes the fiber diameter) and the number of fibers was five in all simulation runs; the ratio of the particles' diameter to the fiber was set to 1; the size of the deposition surface was set to $L \times W = 20\ d_f \times 20\ d_f$ for $Pe > 1$ or $L \times W = 40\ d_f \times 40\ d_f$ for $Pe \leq 1$ (here, *L* and *W* denote the length and the width of deposition surface, respectively).

According to the definition of *Pe* in Section 2.2, a small *Pe* (e.g., $Pe \leq 1$) means that Brownian diffusion is the controlling transport mechanism of particle deposition, while a large *Pe* (e.g., $Pe \gg 1$) means that convection is the dominant transport mechanism. The dust layer's growth was simulated for two typical cases of $Pe = 0.5$ and 5000. The three-dimensional morphologies caused by particle deposition on the surfaces of the fibers in three typical deposition stages are shown in Figure 4.

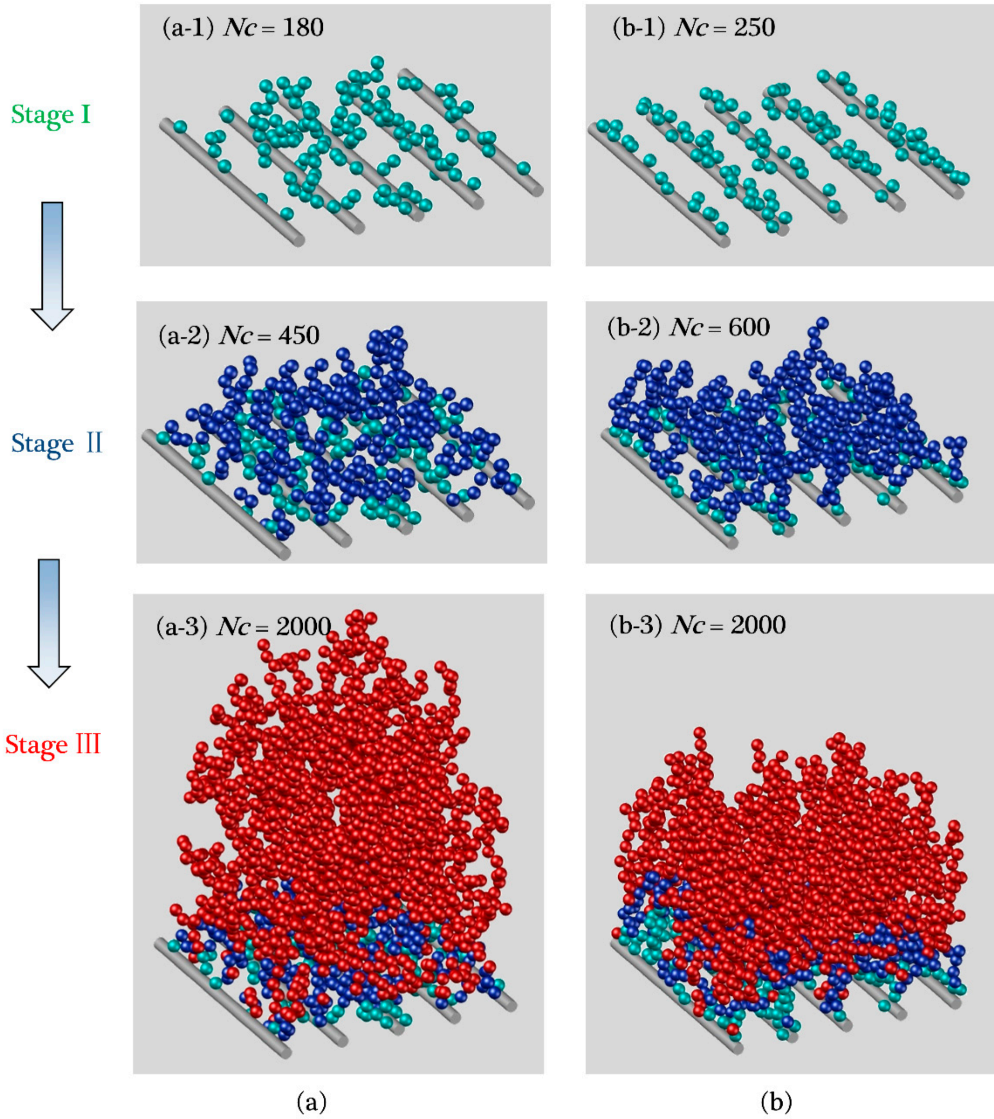

Figure 4. Typical simulated morphological structures of dust layers: (**a**) $Pe = 0.5$; (**b**) $Pe = 5000$.

Figure 4 indicates that the process of particle deposition can be characterized as occurring in three stages, namely the particle adhesion stage (Stage I), the dendrite growth stage (Stage II) and the dust cake growth stage (Stage III). During Stage I, the particles were deposited directly on the fibers' surface, and acted as a new collection point for the deposition of subsequent particles. Following this, a dendritic (or chain-like) particle deposit formed and grew until it interacted with the particle dendrites on the adjacent fibers, eventually forming a porous network-like structure. Finally, the particle deposition process entered the filter cake growth stage. This stage was characterized by the fact that the particles were completely captured by the previously deposited particles, whereas the fiber almost lost the capacity to collect approaching particles.

In addition, significant differences in the morphologies of the dust layers under the two conditions of Pe = 0.5 and 5000 can be observed in Figure 4. When Pe = 0.5 (see Figure 4a), the particle diffusion effect was stronger than advection transportation, and the dust layer grew as a more open and looser structure. It was noted that the dust layer simulated for a small Pe by the present 3D model was different from that characterized as a huge open tree-like morphology in the 2D space [25,34]; this was because the particles' movement in 2D space was geometrically more restricted than that in 3D space and had fewer opportunities to penetrate into the dust layer. For a large Pe (Pe = 5000), a compact dust layer was observed, as shown in Figure 4b.

In order to explain the differences in the deposits' morphologies under different values of Pe, the trajectories of the particles for a set of Pe values were calculated, as shown in Figure 5.

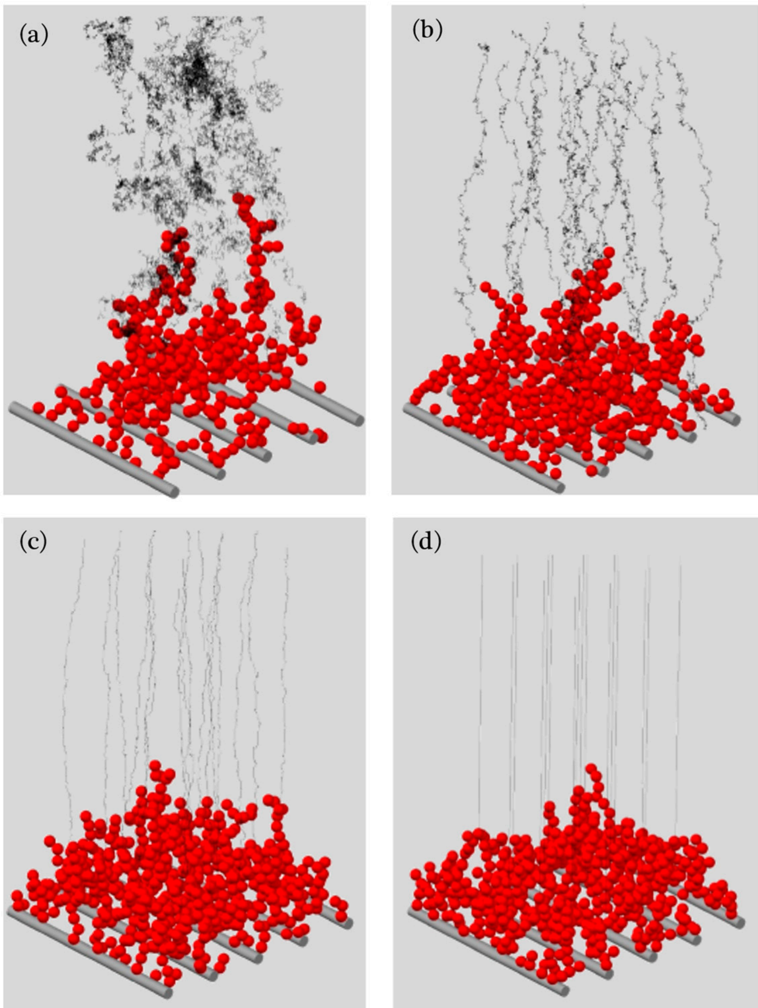

Figure 5. Characteristics of particle trajectories: (**a**) Pe = 0.2; (**b**) Pe = 0.5; (**c**) Pe = 1; (**d**) Pe = 5000.

It can be seen that when *Pe* = 0.2, the particle trajectories showed strong random walk characteristics, which suggested that the particles at the tip of the deposit had a greater opportunity to adhere the incoming particles compared with those at the bottom of the dust layer, and the dust layer grew as a "non-equilibrium" state. However, when *Pe* = 5000, the particle trajectories almost followed the streamline, and the particle transport mechanism was dominated by convection. In this case, the deposition positions of the particles depended on their initial positions. Since the initial positions of the approaching particles were uniformly and randomly distributed, from a statistical point of view, the probability of each point on the dust layer contacting the approaching particles was equal, resulting in a relatively uniform deposition surface. It was thus evident that the transport mechanism plays a crucial role in the evolution of particle deposition morphologies.

3.3. Pore Structure of the Dust Layer

The packing density is an important parameter that describes the pore structure of a dust layer, and it is also a key parameter that affects the filtration pressure drop and other dynamic behaviors of the dust layer (such as dust layer collapse and compression) that are closely related to filtration performance. Therefore, it is necessary to analyze the effect of the particle transport mechanism on the variation in the characteristics of the packing density of the dust layer. The dust layer density ρ_c was defined as the ratio of the total volume of particles in a sampled dust layer to the volume of the dust layer. The height of a particle diameter was taken as the sampling layer thickness along the *y* direction, and then ρ_c could be calculated by:

$$\rho_c(H) = \frac{\sum_{i=1}^{n_p(H)} \pi d_p^3}{L \times W \times d_p} \tag{12}$$

The spatial distributions of the packing densities of dust layers under different *Pe* numbers are given here to observe the pore structure characteristics of the dust layers in detail. The calculation results are shown in Figure 6. The abscissa in the figure represents the dimensionless dust layer's thickness, *H*, which is defined as the ratio of the thickness of the dust layer to the particle diameter d_p.

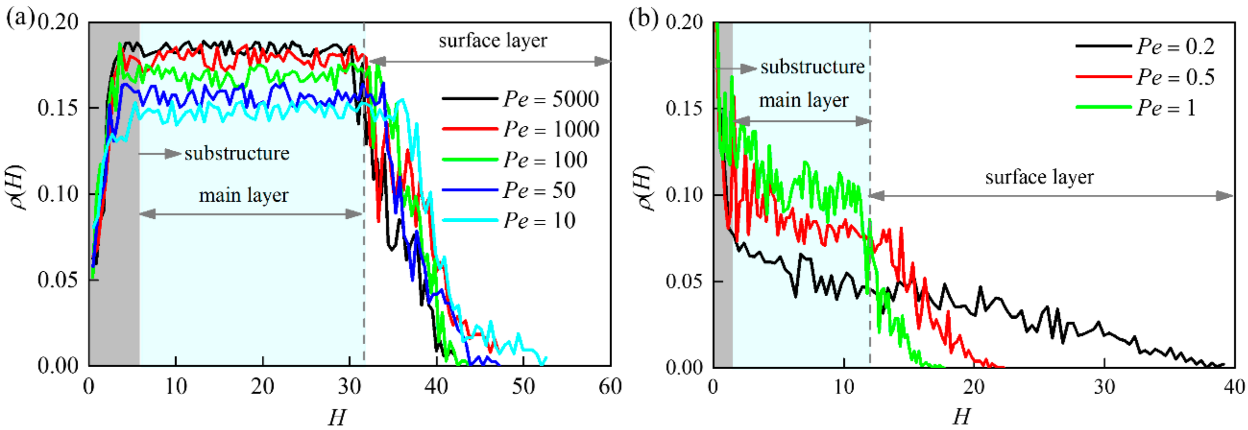

Figure 6. Dust layer density, ρ_c, vs. height, *H*: (**a**) *Pe* > 1; (**b**) *Pe* $\leq$ 1.

Figure 6a shows that for the case of *Pe* > 1, the packing densities of the dust layers first experienced a sharp rise with the increase in the thickness (see the gray area in Figure 6a), then entered a relatively stable stage and finally decreased sharply with the increase in thickness. According to the single fiber filtration theory [49], the efficiency of ultrafine particle collection by the fibers was low for a large *Pe*. As a result, the number of particle dendrites formed on the fiber surface was relatively small, and the number of particles contained in a single particle dendrite was also lower, resulting in a low dust layer density at the bottom of the dust layer. When the particles dendrites grew to a certain height, the number of particles contained in a single particle dendrite increased significantly, leading to an increase in the dust layer density.

Unlike the case of $Pe > 1$, when the transport mechanism of particles evolved to be dominated by diffusion ($Pe \leq 1$), the number of particles captured by the fibers increased significantly based on fibrous filtration theory, leading to a high dust layer density. However, due to the "non-equilibrium" growth of particle dendrites under this condition, larger dendrites had more opportunities to contact the approaching particles and continue to grow, while relatively small dendrites were shielded by the adjacent larger ones from capturing the approaching particles, thereby stopping their growth; this process inevitably caused the dust layers density to decrease as the thickness increased (gray area in Figure 6b). In addition, it can be observed in Figure 6b that with the decrease in *Pe*, the dust layer density in the stable stage gradually decreased with the increase in the thickness of the dust layer.

Although there are differences in the changes in the dust layer density with thickness for different values of *Pe*, the dust layers can still be divided into three typical structures. At the bottom of the dust layer, there was a dust layer structure whose packing density increased or decreased sharply with the height (depending on the particle transportation mechanism), in this study, it was called the "dust layer substructure ", which played a key role in the formation rate and stability of the dust layers. The density of the dust layer above the substructure layer remained relatively stable along the thickness. This layer was called the "main layer" and it mainly contributed to the formation of the filter pressure drop. The area where the dust layer density had a sharp drop was called the "surface layer". It should be pointed out here that the division of the dust layer structure based on the density and the division of these three stages in the process of dust layer growth pertained to the description of different physical problems. The dust layer substructure was the dust layer structure formed by particle adhesion and particle dendrite growth, while the dust layer's main layer and surface layer were the results of dust cake growth.

4. Conclusions

The growth of a dust layer by the convective-diffusive arrival of ultrafine particles in a model filter composed of an array of identical parallel fibers placed transverse to the flow were simulated through an off-lattice Monte Carlo method. The parameter that determined the structure of the dust layer was identified in terms of an appropriate *Pe* number, and the pore structure of dust layer was analyzed. The principal results are as follows:

(1) The particle transport mechanisms (i.e., diffusion and convection) play a key role in determining the morphology of the dust layer. For $Pe \leq 1$, the dust layer grew as a more open and looser structure with a very rough top surface boundary. For $Pe > 1$, convection became the controlling transportation mechanism for particle deposition, resulting in more compact, less porous dust layers.

(2) In the current 3D simulation, a les dense dust layer near the fibrous filtration medium could be observed in the case of $Pe > 1$, owing to not having enough deposition area for particle deposition compared with the wall substrate, whereas for a smaller *Pe* (e.g., $Pe \leq 1$), this phenomenon was not observed.

(3) The dust layer's morphology can be divided into three typical parts of the substructure, the main layer and the surface layer along the direction of dust layer growth. In the substructure, the dust layer's density increased sharply with its thickness for $Pe > 1$ and decreased for $Pe \leq 1$. In the main layer, the density remained relatively constant with the thickness, while in the surface layer, the density decreased sharply for a larger *Pe*.

It should be pointed out that the present simulation model does not take some complex dynamical behaviors of the particle deposition process into account, such as the rebound of impacting particles, or the collapse and re-entrainment of particle dendrites formed on the fiber's surface, whereas these 'secondary' behaviors may occur in the actual filtration process and have a tendency to compress the dust layer, making its porosity reduce. Obviously, a quantitative analysis of these dynamical behaviors requires the van der Waals forces of particle–fiber and particle–particle interactions, and two-way coupling between the gas-deposited particle (or particle dendrites). Moreover, in practical circumstances, particles in dust-laden gas are likely to be nonuniform in size, i.e., a monodisperse particle system. Although it is often possible to approximate polydisperse particles by their average size, dust-laden gas containing particles with the same mean particle size would not necessarily behave in the same way. The particle size distribution is obviously an important factor for particle deposition. In further work, a more real numerical simulation model should be developed to account for these factors and to give greater insights into particles' deposition behavior.

Author Contributions: Conceptualization, S.W. and H.Z.; methodology, H.Z.; software, H.Z. and C.Q.; validation, S.W., H.Z. and Y.C.; formal analysis, S.W.; investigation, Y.C.; resources, C.L. and G.L.; data curation, S.W.; writing—original draft preparation, S.W.; writing—review and editing, S.W., H.Z. and Y.C.; visualization, H.Z., C.L., G.L. and C.Q.; supervision, H.Z.; project administration, H.Z.; funding acquisition, S.W. and H.Z. All authors have read and agreed to the published version of the manuscript.

Funding: This research was funded by the National Natural Science Foundation of China (grant number 51864014), the Natural Science Foundation of Guangxi Zhuang Autonomous Region (grant number 2021GXNSFAA220079), the Natural Science Foundation of Guilin University of Aerospace Technology (grant number XJ20KT13) and the Key Science and Technology Projects in Transportation Industry of the Ministry of Transport, China (grant number 2021-MS5-126).

Institutional Review Board Statement: Not applicable.

Informed Consent Statement: Not applicable.

Data Availability Statement: Not applicable.

Acknowledgments: We would like to thank the editors and reviewers for their key work.

Conflicts of Interest: The authors declare no conflict of interest. The funders had no role in the design of the study; in the collection, analyses, or interpretation of data; in the writing of the manuscript; or in the decision to publish the results.

References

1. Guo, B.; Wang, Y.A.; Zhang, X.Y.; Che, H.Z. Temporal and spatial variations of haze and fog and the characteristics of $PM_{2.5}$ during heavy pollution episodes in China from 2013 to 2018. *Atmos. Pollut. Res.* **2020**, *11*, 1847–1856. [CrossRef]
2. Zhang, T.H.; Lu, B.Q.; Quan, X. $PM_{2.5}$ acidity during haze episodes in Shanghai. *China Environ. Chem.* **2021**, *18*, 168–176. [CrossRef]
3. Manisalidis, I.; Stavropoulou, E.; Stavropoulos, A. Environmental and health impacts of air pollution: A review. *Front. Public Health* **2020**, *8*, 14. [CrossRef]
4. Karmakar, M.K.; Chandra, P.; Chatterjee, P.K. A review on the fuel gas cleaning technologies in gasification process. *J. Environ. Chem. Eng.* **2015**, *3*, 689–702.
5. Thomas, D.; Penicot, P.; Contal, P. Clogging of fibrous filters by solid aerosol particles experimental and modelling study. *Chem. Eng. Sci.* **2001**, *56*, 3549–3561. [CrossRef]
6. Xia, T.; Chen, C. Evolution of pressure drop across electrospun nanofiber filters clogged by solid particles and its influence on indoor particulate air pollution control. *J. Hazard. Mater.* **2021**, *402*, 123479. [CrossRef] [PubMed]
7. Myojo, T.; Kanaoka, C.; Emi, H. Experimental observation of collection efficiency of a dust-loaded fiber. *J. Aerosol Sci.* **1984**, *15*, 483–489. [CrossRef]
8. Payatakes, A.C.; Chi, T. Particle deposition in fibrous media with dendrite-like pattern: A preliminary model. *J. Aerosol Sci.* **1976**, *7*, 85–100. [CrossRef]
9. Payatakes, A.C.; Okuyama, K. Effects of aerosol particle deposition on the dynamic behavior of uniform or multilayer fibrous filter. *J. Colloid Interface Sci.* **1982**, *88*, 55–78. [CrossRef]
10. Kasper, G.; Schollmeier, S.; Meyer, J. The collection efficiency of a particle-loaded single filter fiber. *J. Aerosol Sci.* **2009**, *40*, 993–1009. [CrossRef]
11. Kasper, G.; Schollmeier, S.; Meyer, J. Structure and density of deposits formed on filter fibers by inertial particle deposition and bounce. *J. Aerosol Sci.* **2010**, *41*, 1167–1182. [CrossRef]
12. Calle, S.; Contal, P.; Thomas, D. Evolutions of efficiency and pressure drop of filter media during clogging and cleaning cycles. *Powder Technol.* **2002**, *128*, 213–217. [CrossRef]

13. Song, C.B.; Park, H.S.; Lee, K.W. Experimental study of filter clogging with monodisperse PSL particles. *Powder Technol.* **2006**, *163*, 152–159. [CrossRef]
14. Payatakes, A.C.; Gradoń, L. Dendritic deposition of aerosol particles in fibrous media by inertial impaction and interception. *Chem. Eng. Sci.* **1980**, *35*, 1083–1096. [CrossRef]
15. Payatakes, A.C.; Gradoń, L. Dendritic deposition of aerosols by convective Brownian diffusion for small, intermediate and high particle Knudsen numbers. *AlChE J.* **1980**, *26*, 443–454. [CrossRef]
16. Hosseini, S.A.; Tafreshi, H.V. Modeling particle-loaded single fiber efficiency and fiber drag using ANSYS–Fluent CFD code. *Comput. Fluids* **2012**, *66*, 157–166. [CrossRef]
17. Lindquist, G.J.; Pui, D.Y.H.; Hogan, C.J., Jr. Porous particulate film deposition in the transition regime. *J. Aerosol Sci.* **2014**, *74*, 42–51. [CrossRef]
18. Kulkarni, P.; Biswas, P. A Brownian dynamics simulation to predict morphology of nanoparticle deposits in the presence of interparticle interactions. *Aerosol Sci. Technol.* **2004**, *38*, 541–554. [CrossRef]
19. Mädler, L.; Lall, A.A.; Friedlander, S.K. One-step aerosol synthesis of nanoparticle agglomerate films: Simulation of film porosity and thickness. *Nanotechnology* **2006**, *17*, 4783. [CrossRef]
20. Kim, J.; Shin, J.; Lee, D. Microstructural transition of nanoparticle deposits from multiple dendrites to compact layer. *J. Aerosol Sci.* **2022**, *159*, 105876. [CrossRef]
21. Chen, J.C.; Kim, A.S. Brownian dynamics, molecular dynamics, and Monte Carlo modeling of colloidal systems. *Adv. Colloid Interface* **2004**, *112*, 159–173. [CrossRef]
22. Kanaoka, C.; Hiragi, C.; Tanthapanichakoon, C. Stochastic simulation of the agglomerative deposition process of aerosol particles on an electret fiber. *Powder Technol.* **2001**, *118*, 97–106. [CrossRef]
23. Kanaoka, C.; Emi, H.; Myojo, T. Simulation of the growing process of a particle dendrite and evaluation of a single fiber collection efficiency with dust load. *J. Aerosol Sci.* **1980**, *11*, 377–383. [CrossRef]
24. Kanaoka, C.; Emi, H.; Tanthapanichakoon, W. Convective diffusional deposition and collection efficiency of aerosol on a dust-loaded fiber. *AIChE J.* **1983**, *29*, 895–902. [CrossRef]
25. Veerapaneni, S.; Wiesner, M.R. Particle deposition on an infinitely permeable surface: Dependence of deposit morphology on particle size. *J. Colloid Interface Sci.* **1994**, *162*, 110–122. [CrossRef]
26. Rodríguez-Pérez, D.; Castillo, J.L.; Antoranz, J.C. Relationship between particle deposit characteristics and the mechanism of particle arrival. *Phys. Rev. E* **2005**, *72*, 021403. [CrossRef]
27. Song, J.H.; Choi, K.H.; Dai, R. Controlled kinetic Monte Carlo simulation of laser improved nano particle deposition process. *Powder Technol.* **2018**, *325*, 651–658. [CrossRef]
28. Stöcklmayer, C.; Höflinger, W. Simulation of the filtration behaviour of dust filters. *Simul. Pract. Theory* **1998**, *6*, 281–296. [CrossRef]
29. Jeon, K.J.; Jung, Y.W. A simulation study on the compression behavior of dust cakes. *Powder Technol.* **2004**, *141*, 1–11. [CrossRef]
30. Zhu, H.; Fu, H.M.; Kang, Y.M. Numerical simulation of particles deposition and rebound on fiber surface. *J. Cent. South Univ.* **2013**, *44*, 3086–3094.
31. Tao, R.; Yang, M.; Li, S. Effect of adhesion on clogging of microparticles in fiber filtration by DEM-CFD simulation. *Powder Technol.* **2020**, *360*, 289–300. [CrossRef]
32. Xiong, G.; Gao, Z.; Hong, C. Effect of the rolling friction coefficient on particles' deposition morphology on single fibre. *Comput. Geotech.* **2020**, *121*, 103450. [CrossRef]
33. Li, Y.; Vu, N.; Kim, A.S. 3-D Monte Carlo simulation of particle deposition on a permeable surface. *Desalination* **2009**, *249*, 416–422. [CrossRef]
34. Wu, S.X.; Zhu, H.; Fu, H.M.; Kang, Y.M. Stochastic simulation of convective diffusional deposition of ultrafine particles on surface of fibers. *J. Cent. South Univ.* **2015**, *46*, 4738–4746.
35. Reist, P.C. *Aerosol Science and Technology*, 2nd ed.; McGraw-Hill Press: New York, NY, USA, 1993; pp. 52–65.
36. Li, A.; Ahmadi, G. Dispersion and deposition of spherical particles from point sources in a turbulent channel flow. *Aerosol Sci. Technol.* **1992**, *16*, 209–226. [CrossRef]
37. Yates, J.T.; Johnson, J.K. *Molecular Physical Chemistry for Engineers*; University Science Books Press: Sausalito, CA, USA, 2007; pp. 317–320.
38. Friedlander, S.K. Mass and heat transfer to single spheres and cylinders at low Reynolds numbers. *AIChE J.* **1957**, *3*, 43–48. [CrossRef]
39. Boraey, M.A.; Vehring, R. Diffusion controlled formation of microparticles. *J. Aerosol Sci.* **2014**, *67*, 131–143. [CrossRef]
40. Vehring, R.; Foss, W.R.; Lechuga-Ballesteros, D. Particle formation in spray drying. *J. Aerosol Sci.* **2007**, *38*, 728–746. [CrossRef]
41. Huang, W.G.; Hibbert, D. Fast fractal growth with diffusion, convection and migration by computer simulation: Effects of voltage on probability, morphology and fractal dimension of electrochemical growth in a rectangular cell. *Phys. A* **1996**, *233*, 888–896. [CrossRef]
42. Huang, W.G.; Hibbert, D. Computer modeling of electrochemical growth with convection and migration in a rectangular cell. *Phys. Rev. E* **1996**, *53*, 727–730. [CrossRef]
43. Witten, T.A.; Sander, L.M. Diffusion-limited aggregation. *Phys. Rev. B* **1983**, *27*, 5686. [CrossRef]
44. Meakin, P. Effects of particle drift on diffusion-limited aggregation. *Phys. Rev. B* **1983**, *28*, 5221–5224. [CrossRef]

45. Kuwabara, S. The forces experienced by randomly distributed parallel circular cylinders or spheres in a viscous flow at small reynolds numbers. *J. Phys. Soc. Jpn.* **1959**, *14*, 527–532. [CrossRef]
46. Henry, F.; Ariman, T. Cell model of aerosol collection by fibrous filters in an electrostatic field. *J. Aerosol Sci.* **1981**, *12*, 91–103. [CrossRef]
47. Kanaoka, C.; Emi, H.; Hiragi, S.; Myojo, T. The Morphology of Particle Agglomerates on a Fiber When Inertia and Interception are Predominant Collection Mechanisms. *J. Soc. Powder Technol. Jpn.* **1987**, *24*, 74–80. [CrossRef]
48. Bhutra, S.; Payatakes, A.C. Experimental investigation of dendritic deposition of aerosol particles. *J. Aerosol Sci.* **1979**, *10*, 445–464. [CrossRef]
49. Lee, K.W.; Liu, B.Y.H. Theoretical study of aerosol filtration by fibrous filters. *Aerosol Sci. Technol.* **1982**, *1*, 147–161. [CrossRef]